Capillary origami controlled by an electric field†

Miguel Piñeirua,* José Bico and Benoît Roman

Received 18th February 2010, Accepted 12th April 2010
DOI: 10.1039/c0sm00004c

We show experimentally how an electric field can control the folding and unfolding of a thin elastic membrane around a liquid droplet. As the voltage is increased above a critical value the membrane unfolds completely. The transition is reversible, although the structure closes back for a lower critical tension. We propose scaling laws for these critical voltages based on the interaction between surface tension, elastic and electric energies. These scaling laws are in qualitative agreement with experiments and a simplified 2D simulation of the problem, providing a useful tool for designing practical micro-devices actuated by an electric field.

1 Introduction

Recent studies have shown how capillary forces can be used to fold thin sheets in a controlled way and thus to produce 3D microscale objects.[1–5] As an example of a practical application, Gua *et al.* have developed 3D photovoltaic cells with enhanced efficiency by wrapping thin Si foils around water droplets.[6] This technique takes advantage of dominating surface tension forces at small scales making it possible to wrap thin elastic sheets around droplets. A wide range of 3D shapes can be obtained if the initial planar patterns of the elastic sheets are properly tuned.[1] However, for different applications such as micro-actuators or digital displays, it would be interesting to have the possibility of switching between the closed and opened states at will, for instance using an electric signal.

Indeed, the use of electric fields provides an efficient way of manipulating liquid droplets without the use of mechanical moving parts. For example, a simple way of modifying the wetting properties of liquids is electrowetting, whose physical basis was first described at the end of the 19th century by Lippmann.[7] In recent years, EWOD (electrowetting over dielectrics[9,8]) has been used in a wide variety of applications, ranging from microlenses using drops of tunable shape and focal length,[10] to the manipulation of micro droplets in lab-on-a-chip devices[13,11] and capillary driven motors.[12] In these 'static electrowetting' cases,[14] the effect of an electric field can be viewed as changing the effective macroscopic contact angle.[15]

In the present work we ask if an electric field can be used to actuate the closure and reopening of a capillary origami. Since capillary forces induce wrapping, we need an additional force (electrostatics) acting against surface tension to promote the reopening of the structure. We emphasize that this situation, with a contact line pinned at the edges of a flexible dielectric, is however different from classical static electrowetting where the liquid contact line moves on a rigid dielectric layer.

We first describe the relevant physical parameters in the interaction between elastic, surface tension and electric forces. In the second part experimental results are presented, discussed and compared with a 2D numerical model of the system. We finally give scaling arguments for the opening and closing conditions.

2 Characteristic scales

In the problem of spontaneous wrapping of elastic sheets around droplets, the deformations of the sheet reduce the contact area between the droplet and air, thus decreasing the surface tension energy by a quantity of the order of γL^2 (γ being the surface tension between the liquid and air and L the typical length of the sheet). This reduction in surface tension energy is balanced by an increment of bending energy in the elastic membrane. For a thin plate, the isometric bending energy per unit surface is defined locally by $B\kappa^2/2$, where κ is the curvature and $B = Eh^3/12(1-\nu^2)$ is the bending stiffness of the plate (E being the Young's modulus, ν is the Poisson's ratio and h is the thickness). As a consequence, spontaneous wrapping is expected when surface energy overcomes the bending energy corresponding to $\kappa \sim 1/L$:

$$\frac{B}{L^2} L^2 < \gamma L^2 \tag{1}$$

A characteristic length of this problem can be defined as

$$L_{EC} = \sqrt{\frac{B}{\gamma}} \tag{2}$$

known as the *elastocapillary length*.[16] This scaling argument indicates that the critical length L_{crit} beyond which the elastic membrane totally wraps the droplet should be proportional to L_{EC}. For instance, in the work done by Py *et al.*,[1] triangular sheets of side length L were experimentally found to form pyramids for $L > 11.9L_{EC}$.

The addition of an electric field, as shown in Fig. 1, leads to electric forces that are expected to counteract surface tension.

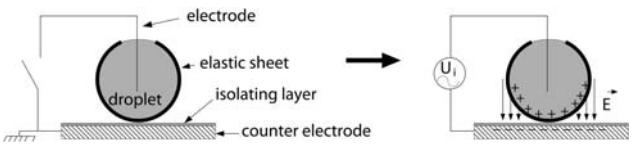

Fig. 1 Sketch of the experimental setup.

Physique et Mécanique de Millieux Hétérogènes, UMR 7636 CNRS ESPCI-UPMC-Paris 7, 10 rue Vauquelin, 75231, Paris CEDEX 5, France. E-mail: pineirua@pmmh.espci.fr

† Electronic supplementary information (ESI) available: Supplementary movie. See DOI: 10.1039/c0sm00004c

Indeed, for an opened structure the capacitance of the system can be approximated to that of a parallel plate system,[15] which leads to an electric energy $E_e = \epsilon L^2 U^2/2(d + h)$, where ϵ and d are the dielectric constant and the thickness of the insulating layer, respectively (we assume that both layers have the same dielectric constant). The comparison between surface tension and electric energies yields the characteristic voltage:

$$U_0 = \sqrt{\frac{\gamma(d+h)}{\varepsilon}} \quad (3)$$

beyond which electric forces are expected to overcome surface tension. In our experiments the physical parameters are of the order of $\gamma \simeq 72$ mN m^{-1}, $h \sim 50$ μm, $d \sim 60$ μm, $\epsilon \sim 4.4 \times 10^{-11}$ F/m, which leads to $U_0 \sim 800$ V. This high value can however be considerably reduced in practical applications if the thicknesses of the dielectric layers are scaled down to a few microns.

3 Experimental setup

The experimental setup used to generate the electric field between the droplet and the substrate is sketched in Fig. 1. The AC voltage is generated with a Tektronik 1254 signal generator, amplified with a Trek 8654 high voltage amplifier. The electrodes consist of a 10 μm diameter copper wire (immersed in the droplet) and a 5 mm thick brass plate (counter electrode). To avoid electrical short circuit between the electrodes in case of accidental water spilling, the counter electrode is covered with a strip of adhesive tape (insulating layer) of thickness $d = 60$ μm. In order to improve the droplet conductivity, experiments were carried out using water with a 0.3% of salt concentration. Membranes were made of polydimethylsiloxane (PDMS, Dow corning Sylgard 1 : 10 and 1 : 20 polymer/curing agent mix) spin coated at rotating speeds of 1000–3500 rpm, over Emery polishing paper 2/0 with a measured average roughness $R_a = 4.24$ μm. Spin coating over rough surfaces leads to rough sided membranes, which significantly reduces the adhesion of the membranes on the insulating layer. To proceed with the experiment, triangular shapes of side length L were cut out from the PDMS sheets of different thicknesses varying from 60 μm < h < 100 μm. A droplet of salty water 5–30 μl is then deposited over the initially flat PDMS shape. As shown by Py *et al.*,[1] the elastic sheet spontaneously wraps the droplet if $L > L_{crit} \sim L_{EC}$. Once the origami is formed, the copper wire electrode is immersed inside the droplet. A 1 kHz AC voltage is imposed between the electrodes and increased gradually from 0 V until the origami has completely reopened. The voltage is then decreased at the same rate until the origami closes again. Images of the evolution of the origami are taken during the experiments at 10 frames per second, as well as simultaneous recordings of the voltage between the electrodes and the capacitance of the droplet–membrane system.

4 Results and discussion

4.1 Experimental results

A series of images obtained during a typical experiment is shown in Fig. 2 (see also ESI†). These first results reveal that it is possible to open the closed origami structure if a sufficiently strong electric field is imposed between the droplet and the counter electrode. The images in Fig. 2-a show the evolution of the unwrapping as the voltage between the electrodes is increased. The membrane starts to open gradually until a critical voltage is reached: one corner of the triangle suddenly jumps over

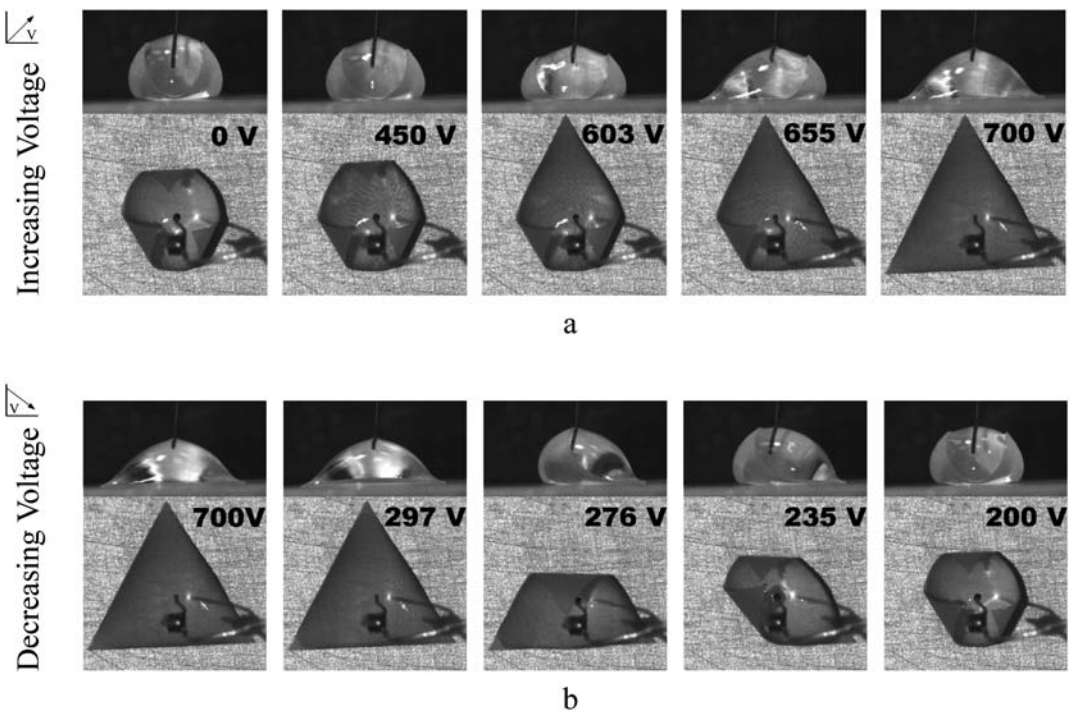

Fig. 2 Images of the lateral and upper views obtained during the experiments, (a) increasing voltage, (b) decreasing voltage. $L = 7$ mm, $h = 80$ μm, $d = 60$ μm and $L_{EC} = 0.47$ mm.

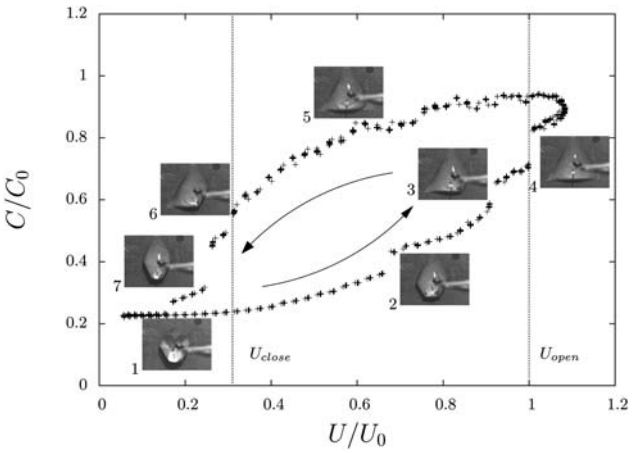

Fig. 3 Measurements of the system's capacitance as a function of the applied voltage for 5 continuous cycles with $L/L_{EC} = 13.5$, $h = 80$ μm and $d = 60$ μm. $C_0 = 6.66$ pF is the capacitance for a parallel plate system of triangular surface with $L = 7$ mm. $U_0 = 857.2$ V.

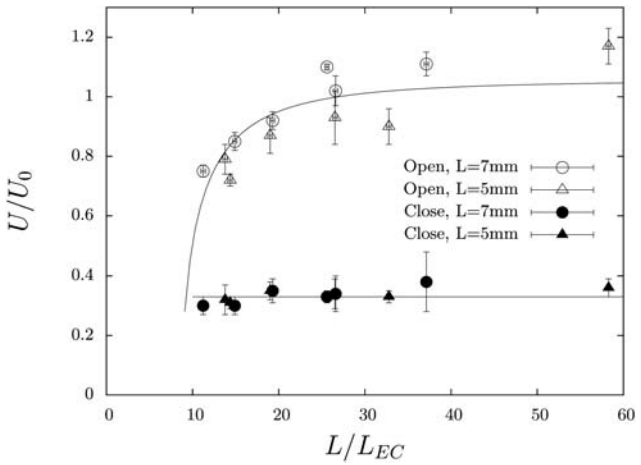

Fig. 4 Experimental results for U_{open} and U_{close} as a function of L/L_{EC}. Solid lines show the fit of the experimental data to expressions obtained for U_{open} and U_{close} from the scaling analysis developed in section 4.2.2, see eqn (9).

the counter electrode. Similar jumps are successively observed as the voltage is progressively increased. We define as U_{open} the RMS value of the voltage beyond which the membrane lies flat over the counter-electrode (last image in Fig. 2-a). A further increase in the voltage does not induce any modification of the shape. However, tiny droplets are ejected when high voltages are reached (typically 1 kV in our experiments) as commonly observed in classical electrowetting experiments.[15] This extreme situation would not be desired for practical applications as it may lead to electrical shortcuts and to the adhesion of the membrane on the counter-electrode. Once U_{open} is reached, the voltage is progressively decreased. Contrary from what would be expected from a continuous transition, the sheet remains flat until one corner suddenly folds at a voltage defined as U_{close} (third image in Fig. 2-b), significantly lower than U_{open}. As the voltage is decreased, the two remaining corners successively fold in the same sudden way and the origami structure recovers its initial shape. To illustrate the hysteresis we measured the capacitance of the system for a complete cycle. These measurements are presented in Fig. 3.The capacitance of the system is expected to be proportional to the surface at contact between the origami and the counter electrode. Besides illustrating the hysteresis in the cycle, the measurement of the capacitance also gives some information of the opening and closing processes. As commented before, when the voltage starts to increase the membrane begins to unwrap in a very slow and continuous way. This unwrapping process corresponds to the continuous increment in the system capacitance between points 1 and 2 in the cycle shown in Fig. 3. Then the sudden unwrapping of one of the corners occurs, and appears as a discontinuous jump of the capacitance in point 2. The membrane keeps opening gradually until the second corner and finally the third corner opens generating discontinuous jumps of the capacitance in points 3 and 4, respectively. After completely opening (point 4), we would expect the capacitance to remain constant until the first corner closes again. However, during the decrease in voltage, dewetting can be observed near the corners of the triangle, which leads to a reduction in the system's capacitance (point 5). Once the electric field is too weak to hold the opened state, a first corner wraps around the droplet

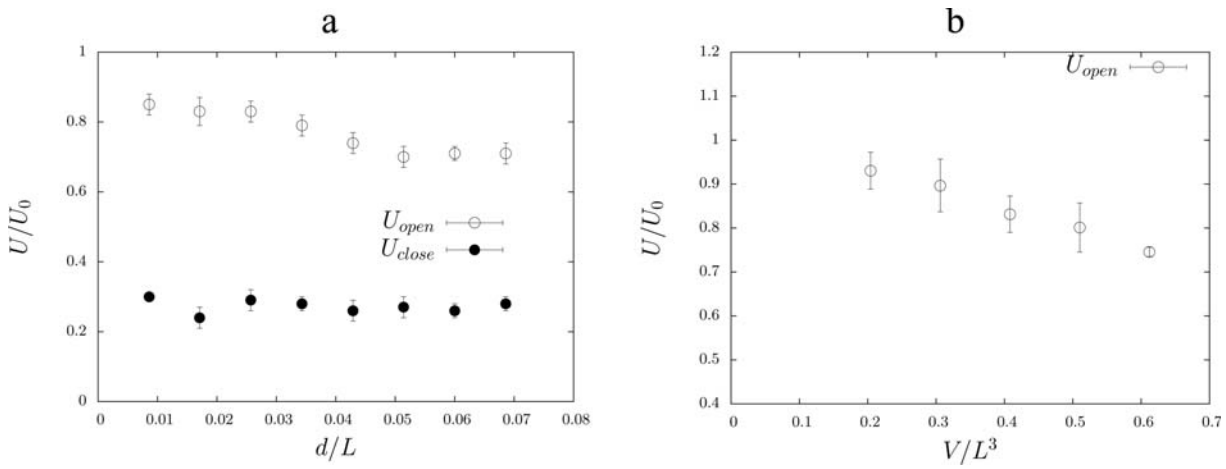

Fig. 5 (a) Experimental results for U_{open} and U_{close} as a function of the thickness of the insulating layer d, for $L/L_{EC} = 13.5$. (b) Experimental results for U_{open} as a function of the droplet volume V for $L/L_{EC} = 13.5$.

again and the value of the capacitance falls in a discontinuous jump at point 6 (this defines the closing voltage U_{close}). The same scenario occurs for the other two corners until the origami is completely closed, moment in which the capacitance returns to its initial value, about five times smaller than the value for the completely opened state.

Different experiments were done varying the experimental parameters, which include the variation of the size of the triangle L, the thickness of the membrane h, the Young modulus of PDMS E, the thickness of the insulating layer d and the ratio V/L^3 (V is the volume of the droplet). Experimental results obtained for U_{open} and U_{close} as a function of L/L_{EC} for fixed values of $d = 50$ μm and $V/L^3 = 0.058$ are shown in Fig. 4. The plotted measurements present clearly the hysteresis between the opening and closing voltages. The collapse of the data in this graph confirms that U_0 and L_{EC} are the relevant parameters in the problem. U_0 also gives a good estimate of the voltages found in the experiments. But as shown in Fig. 4, U_{open}/U_0 increases with function of L/L_{EC} and eventually tends to reach a saturation value. Indeed the results obtained by Py *et al.*[1] show that the bending energy is higher for lower values of L/L_{EC}, which promotes the opening of the structure. Conversely the bending energy becomes negligible for high values of L/L_{EC}, which explains the asymptotic regime observed: the opening and closing voltages should only rely on a balance between surface tension and electric energy and not depend on L/L_{EC} anymore. On the other hand, we observe that the closing voltage U_{close}/U_0 remains practically constant and does not seem to depend on L/L_{EC}. Indeed, as the membrane is completely open there is no elastic energy in the system, so the closing process should depend only on the electric field-surface tension interactions, in which the ratio L/L_{EC} does not play any role.

Fig. 5 a shows different experimental results where the thickness of the insulating layer was increased over one order of magnitude while L/L_{EC} and the ratio V/L^3 were kept constant. The ratio U_{open}/U_0 appears to decrease slowly as a function of the dielectric thickness d, while U_{close}/U_0 remains constant as it did as a function of L/L_{EC}. Nevertheless, the hysteresis between U_{open} and U_{close} remains large. Additionally, U_{open}/U_0 decreases as a function of the ratio between the droplet volume V and L^3, as shown in Fig. 5 b (in this case the length of the membrane L is kept constant while the volume of the droplet was varied from 10 to 30 μl). As shown by Py *et al.*, the distance between the tips of the wrapped membrane increases with the volume of the droplet. We could then expect to need a lower voltage to open a partially folded membrane compared to the completely closed state. Experimental trends are therefore in agreement with the analysis of the physical parameters. However a more detailed analysis of the problem is required to understand and predict the dependency of the opening and closing voltages as a function of the different experimental parameters. A 2D numerical approach and simplified scaling laws for the opening and closing voltages are presented in the following section.

4.2 2D model and numerical simulations

We consider a simplified 2D model of the system inspired by a recent work from de Langre *et al.*[17] The model consists of a two dimensional system, of width w, formed by the elastic membrane and a liquid–air interface (Fig. 6). The membrane is considered to have a constant length L and a uniform radius of curvature R_1. The radius of curvature of the liquid–air interface R_2 is also considered uniform. The droplet is taken as a conductive body of area S separated from the counter electrode by a dielectric layer of thickness d.

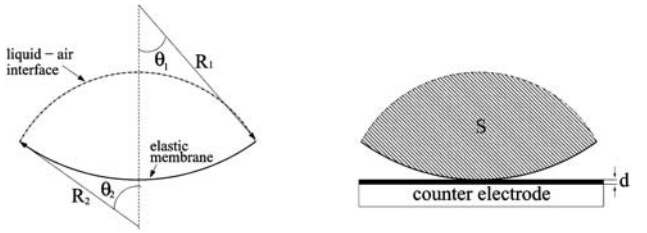

Fig. 6 Sketch of the system used in the 2D simulation: the radii of curvature of the liquid interface, R_1 and of the elastic membrane, R_2, are assumed to be uniform.

The total energy of the system considering the elasticity of the membrane, surface tension and the electric field is given by the following expression:

$$E_t = \frac{BwL}{2R_1^2} + \gamma wL - \sqrt{2}\epsilon w\left(\frac{R_1}{d+h}\right)^{1/2}\arctan\left(\frac{L}{\sqrt{8R_1(d+h)}}\right)U^2 \quad (4)$$

The third term in the last equation approximates the electric energy E_e of a 2D capacitor where one of the electrode is planar, and the other one is a portion (with length L) of cylinder with-curvature R_1. Indeed, if the variations of the gap are small $L^2/R \ll t$ compared to the minimal gap $t = d + h$, the portion of cylinder can be considered as planar and we find the usual formula for parallel plates $E_e = -\epsilon wLU^2/2t$. Conversely in the opposite case $L \gg \sqrt{R_1 t}$ the energy is almost that of a complete cylinder separated of a plane by a gap t, and we find that E_e reduces to the classical value[18] $E_e = -\pi\epsilon wU^2\sqrt{R_1/2t}$ (valid for $t \ll R_1$).

To carry out the numerical simulations with the 2D model we impose as fixed parameters the non-dimensional values $(d + h)/L$, S/L^2 and L/L_{EC}, for the voltage, dielectric and membrane thicknesses, droplet cross section and membrane length, respectively. For each set of parameters the shape of the system which minimizes the total energy is computed as a function of κ (κ is the curvature $1/R_1$). Fig. 7 shows the results of the simulation for U_{open} and U_{close} as a function of the different parameters. The results for U_{open} as a function of L/L_{EC} agree qualitatively with experiments. As in the experiments, the simulation results for U_{close} are independent of L/L_{EC}. Similarly the simulation shows a decreasing value of U_{open} as a function of the insulating layer thickness d. However, the dependence of U_{close} on d shows a large discrepancy between the simulation and the experiments. This discrepancy is discussed in more detail in the following section. Finally, the opening critical voltage decreases as the volume (or its 2D analog S/L^2) increases in the experiments (Fig. 5-b) as well as in the simulation (Fig. 7-c). The results of the simulation are encouraging since they provide a qualitative agreement with the experiments. Analytical expressions, even approximative, are however more useful for practical applications. In the following

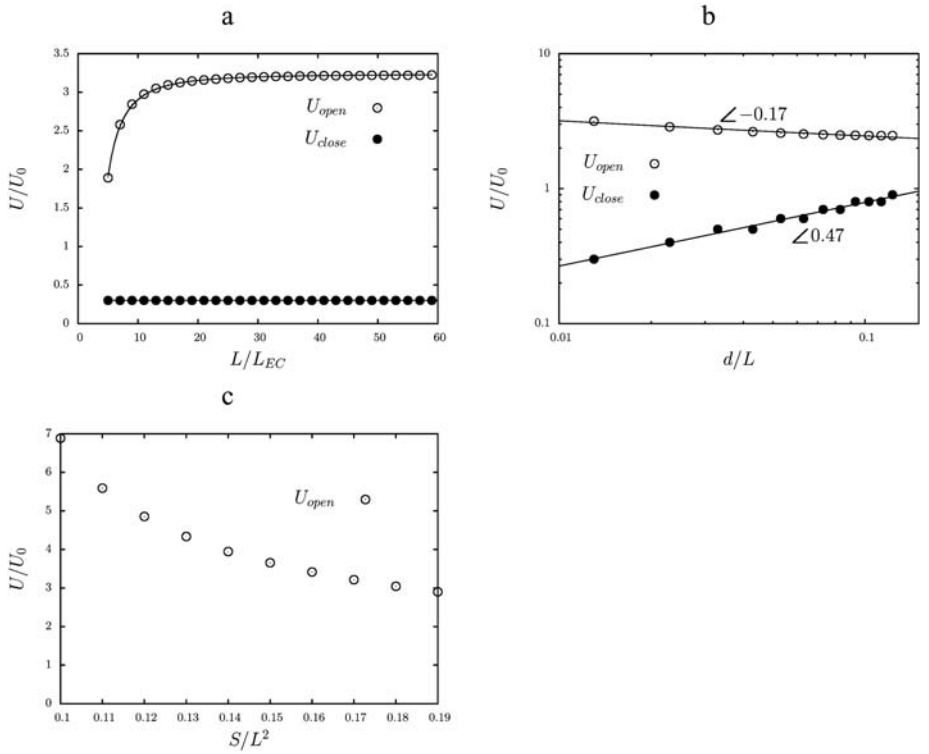

Fig. 7 (a) 2D simulation results for U_{open} and U_{close} as a function of L/L_{EC}, solid lines show the fit of the experimental data to expressions obtained for U_{open} and U_{close} from the scaling analysis in section 5, (b) simulation results as a function of the insulating layer thickness, (c) as a function of S/L^2.

section we derive scaling laws for U_{open} and U_{close} as a function of the physical parameters.

5 Scaling analysis

Based on the same simplified 2D configuration, we first consider the state when the membrane completely wraps the droplet, such that $L \sim \pi R_1$. This state is expected to remain closed while the following torque inequality is verified:

$$\Gamma_\gamma > \Gamma_B + \Gamma_E \tag{5}$$

where Γ_γ, Γ_B and Γ_E are the torques generated by surface tension, bending and electrical forces respectively. The torques due to elastic bending and surface tension are, considering $L \sim R_1$:

$$\Gamma_B \sim \frac{Bw}{R_1} \sim \frac{Bw}{L} \sim \frac{\gamma L_{EC}^2 w}{L} \tag{6}$$

$$\Gamma_\gamma \sim \gamma L w \tag{7}$$

In order to estimate the torque produced by the electric field we consider the electric energy of the system as the energy of a classical cylinder-plane configuration,[18] $E_e = -\pi\epsilon w\sqrt{R_1/2(h+d)}\ U^2$ (valid under condition $R_1 \gg h+d$). The torque due to the electric force is deduced from the derivative $\partial E_e/\partial\theta_1$ where θ_1 is defined on Fig. 6. Considering the geometrical relation $L = R_1\theta_1$, we find:

$$\Gamma_E \sim \frac{\partial E_e}{\partial \theta_1} \sim \varepsilon w \frac{R_1}{L}\sqrt{\frac{R_1}{h+d}}\ U^2 \sim \varepsilon w\sqrt{\frac{R_1}{h+d}}\ U^2 \tag{8}$$

The following expression for U_{open} can finally be inferred from balancing the three torques from eqn (5):

$$U_{open} = \alpha U_0\left(1 - \left(\frac{\beta L_{EC}}{L}\right)^2\right)^{1/2}\left(\frac{L}{h+d}\right)^{1/4} \tag{9}$$

where α and β are numbers expected to be of order 1. Proceeding in a similar way, we compare the torques needed to keep the fully open state to estimate U_{close}. Since the membrane is completely flat, there is no torque generated by the elastic sheet ($\Gamma_b = 0$), which leads to the following condition:

$$\Gamma_E > \Gamma_\gamma. \tag{10}$$

This condition can be rewritten as

$$\frac{\varepsilon}{(d+h)^2} w L^2 U^2 > \gamma w L \tag{11}$$

where the torque is directly computed on the parallel plate configuration. From eqn (11) the following expression for U_{close} can easily be found:

$$U_{close} = U_0\sqrt{\frac{d+h}{L}} \tag{12}$$

which is independent from bending stiffness. It is important to notice that U_{open} will always be larger than U_{close} as soon as $(d + h) << L$ (condition which is also needed to keep valid the

expression obtained for U_{open}). Therefore hysteresis will be present in the system.

To verify the proposed scaling laws we compared them with the experimental data and with the results obtained by numerical simulations carried out with the 2D model. In our experiments we note that the factor $(L/(d+h))^{1/4}$ remains between 2.4 and 2.7 due to the weak exponents. The experimental results for U_{open}/U_0 shown in Fig. 4 were therefore fitted to an expression of the form $f = a\sqrt{1-(\beta L_{EC}/L)^2}$ corresponding to the scaling presented in eqn (9), where $a = \alpha(L/(d+h))^{1/4}$. A fair agreement was found between the experiments and the scaling law in this case. The fitted value obtained $a = 1.11$ shows that α is of order one in eqn (9). On the other hand, we found $\beta \sim 9.22$, which is close to the value of $L/L_{EC} = 11.9$ obtained for triangular shapes by Py *et al.*[1] when $U = 0$ and within the interval $\sqrt{2}\pi < L/L_{EC} < \sqrt{8}\pi L_c/L_{EC}$ proposed by de Langre *et al.*[17] as a wrapping criteria. Also in agreement with eqn (12), in the results shown in Fig. 4, U_{close}/U_0 remains independent of L/L_{EC} with a constant value ~ 0.35. For the same parameters eqn (12) suggests a value of $0.136 < \sqrt{(d+h)/L} < 0.178$. This agreement between the experimental results and the proposed scaling law derived from the 2D model, confirms the hypothesis that elasticity does not play an important role in determining the value of U_{close}.

As shown in Fig. 5-a, U_{open}/U_0 slightly decreases as a function of d. This variation may be approximated in order of magnitude to the expected $((h+d)/L)^{-1/4}$ obtained from the 2D model. However, in the numerical simulation shown in Fig. 7-b, U_{open}/U_0 decreases as $(d/L)^{-0.17}$ and not as $(d/L)^{-0.25}$ as proposed by the scaling law. This difference is due to the relation used to estimate the electric energy which is only valid for $R_1 >> h + d$. However this condition is not verified for the range of d/L range presented in Fig. 7-b (the same range was used in the experiments), which leads to a lower dependence of U_{open}/U_0 on the dielectric thickness.‡ On the other hand, in the experimental results shown in Fig. 5-a, U_{close}/U_0 is independent from the thickness of the insulating layer, which does not agree with the $((d+h)/L)^{1/2}$ scaling law (eqn (12)). This scaling is however verified by the numerical simulations with the 2D model (Fig. 7-b). We believe that the mismatch between the experimental results and the proposed scaling law may be due to the existence of some remaining adhesion between the elastic membrane and the insulating layer of the electrode, in addition to gravity effects. However a better control of the adhesive properties of the membrane and the miniaturization of the system would reduce these effects.

6 Conclusions

We have proven experimentally the feasibility of actuating a capillary origami structure by means of electric forces, being able to switch between its completely opened and closed states in a controlled and reproducible way. A simplified 2D simulation of the problem and scaling laws describing the interaction between surface tension, bending stiffness and electric forces provide qualitative agreement with the experimental results. However a more quantitative description of the actuation would require an improved simulation including three dimensional and gravity effects. From a practical point of view, the use of thinner insulating layers and membranes will result in reduced values for the operating voltages. This system is therefore relatively easy to set up (no moving mechanical parts) at micro-scale, and could provide the basis for a micro-actuator.

‡ An extra simulation was carried out with a range where d/L was small enough to hold the relation $R_1 >> d + h$, which successfully verified the scaling law.

Acknowledgements

We wish to thank Fabien Closa, Charlotte Py, Leatitia Girault and Lionel Agostini for carrying out successfully the preliminary experiments. We also thank Joost van Honschoten for motivating discussions. This work was partially supported by the French ANR Jeunes Chercheurs MecaWet grant and by the Secretaría de Educación Pública (SEP, México).

References

1 C. Py, P. Reverdy, L. Doppler, J. Bico, B. Roman and C. N. Baroud, Capillary origami: spontaneous wrapping of a droplet with an elastic sheet, *Phys. Rev. Lett.*, 2007, **98**, 156103.
2 T. Leong, P. Lester, T. Koh, E. Call and D. Gracias, Surface tension-driven self-folding polyhedra, *Langmuir*, 2007, **23**, 8747–8751.
3 D. Gracias, V. Kavthekar, C. Love, K. Paul and G. Whitesides, Fabrication of micrometer-scale, patterned polyhedra by self-assembly, *Adv. Mater.*, 2002, **14**, 235–238.
4 R. Syms, E. Yeatman, V. Bright and G. Whitesides, Surface tension-powered self-assembly of microstructures- The sate of the art, *J. Microelectromech. Syst.*, 2003, **12**, 387–417.
5 P. Green, R. Syms and E. Yeatman, Demonstration of three-dimensional microstructure self-assembly, *J. Microelectromech. Syst.*, 1995, **4**, 170–176.
6 X. Guo, H. Li, B. Ahn, E. Duoss, J. Hsia, J. Lewis and R. Nuzzo, Two- and three-dimensional folding of thin film single-chrystalline silicon for photovoltaic power applications, *Proc. Natl. Acad. Sci. U. S. A.*, 2009, **106**, 20149–20154.
7 G. Lippmann, Relations entre les phénomènes électriques et capillaires, *Ann. Chim. Phys.*, 1875, **5**, 494–549.
8 J. H. Song, R. Evans, Y. Lin, B. N. Hsu and R. B. Fair, A scaling model for electrowetting-on-dielectric microfluidic actuataors, *Microfluid. Nanofluid.*, 2009, **7**, 75–89.
9 B. Berge, Electrocapillarité et mouillage de films isolants par l'eau, *C.R. Acad. Sci. II*, 1993, **317**, 157–163.
10 B. Berge and J. Peseux, Variable focal lens controlled by an external voltage: an application of electrowetting, *Eur. Phys. J. E*, 2000, **3**, 159–163.
11 M. G. Pollack, A. D. Shenderov and R. B. Fair, Electrowetting-based actuation of droplets for integrated microfluidics, *Lab Chip*, 2002, **2**, 96–101.
12 A. Takei, K. Matsusmoto and I. Shomoyama, Capillary motor driven by electrowetting, *Lab Chip*, 2010, DOI: 10.1039/c001211d.
13 P. Paik, V. K. Pamula and R. B. Fair, 2003, Rapid droplet mixers for digital microfluidic systems, *Lab Chip*, 2003, **3**, 253–259.
14 L. Yeo and H. Chang, Static and spontaneous electrowetting, *Mod. Phys. Lett. B*, 2005, **19**, 549–569.
15 F. Mugele and J. C. Baret, Electrowetting: from basics to applications, *J. Phys.: Condens. Matter*, 2005, **17**, R705–R774.
16 J. Bico, B. Roman, L. Moulin and A. Boudaoud, Elastocapillary coalescence in wet hair, *Nature*, 2004, **432**, 690(2004).
17 E. de Langre, C. N. Baroud and P. Reverdy, Energy criteria for elasto-capillary wrapping, *Journal of Fluids and Structures*, 2010, **26**, 205–217.
18 N. Ida, *Engineering Electromagnetics*, 2nd edn, 2004, Springer, New York.

